

Dynamics of Glass Forming Liquids with Randomly Pinned Particles

Saurish Chakrabarty¹, Smarajit Karmakar^{2,*}, and Chandan Dasgupta^{1,3}

¹Centre for Condensed Matter Theory, Department of Physics, Indian Institute of Science, Bangalore, 560012, India

²TIFR Center for Interdisciplinary Science, Narsingi, Hyderabad 500075, India

³Jawaharlal Nehru Centre for Advanced Scientific Research, Bangalore 560064, India.

*smarajit@tifrh.res.in

ABSTRACT

It is frequently assumed that in the limit of vanishing cooling rate, the glass transition phenomenon becomes a thermodynamic transition at a temperature T_K . However, with any finite cooling rate, the system falls out of equilibrium at temperatures near $T_g (> T_K)$, implying that the very existence of the putative thermodynamic phase transition at T_K can be questioned. Recent studies of systems with randomly pinned particles have hinted that the thermodynamic glass transition may be observed in simulations and experiments carried out for liquids with randomly pinned particles. This expectation is based on the results of approximate calculations that suggest that the temperature of the thermodynamic glass transition increases as the concentration of pinned particles is increased and it may be possible to equilibrate the system at temperatures near the increased transition temperature. We test the validity of this prediction through extensive molecular dynamics simulations of two model glass-forming liquids in the presence of random pinning. We fit the temperature-dependence of the structural relaxation time to the Vogel-Fulcher-Tammann form that predicts a divergence of the relaxation time at a temperature T_{VFT} and identify this temperature with the thermodynamic transition temperature T_K . We find that T_{VFT} does not show any sign of increasing with increasing concentration of pinned particles. The main effect of pinning is found to be a rapid decrease in the kinetic fragility of the system with increasing pin concentration. Implications of these observations for current theories of the glass transition are discussed.

Introduction

The glass transition is characterized by a rapid increase of the viscosity (η) and the structural relaxation time (τ_α) with decreasing temperature.¹⁻⁴ Recent progress⁵⁻¹⁶ in understanding various dynamical aspects of this phenomenon has shed some light on this subject, but the question of whether an “ideal” thermodynamic glass transition, signaled by the vanishing of the configurational entropy density, can occur at a temperature lower than the experimentally defined (dynamic) glass transition temperature remains unanswered. Recently, it was proposed in Ref.,¹⁷ that the difficulty in observing the putative ideal glass transition in simulations and experiments can be bypassed by considering liquids in the presence of quenched disorder and studying the effects of varying disorder strength on the thermodynamic and dynamic properties of the liquid. It was argued from Mean Field (MF) and Renormalization Group (RG) calculations, that a thermodynamic glass transition at a temperature higher than the transition temperature of the liquid without disorder can be achieved by increasing the strength of the quenched disorder in the system. These studies assumed that the Random First Order Transition (RFOT) theory,³⁻⁵ which is currently the most popular theoretical framework for describing equilibrium and dynamic properties of glass-forming liquid near the glass transition, remains valid in the presence of quenched disorder. However, the validity of the RFOT description is still controversial. An alternative description¹⁸ of glassy dynamics, based on the behavior of kinetically constrained systems, does not show¹⁹ the occurrence of a transition at a non-zero temperature with increasing disorder strength. Therefore, a numerical investigation of whether this transition actually occurs in model glass-forming liquids would help in determining which of these competing theories is better at describing structural glasses. The possibility of observing a thermodynamic glass transition in simulations and experiments relies on the theoretically predicted increase of the transition temperature with increasing strength of pinning. It would be interesting to check by simulations whether this prediction is valid for three-dimensional glass-forming liquids. A numerical study of glassy behavior in pinned liquids would also help in understanding the results of a recent experiment²⁰ on colloidal systems with the kind of pinning disorder considered in the theoretical studies.

Existing simulation results for the effects of quenched disorder on the dynamics of supercooled liquids^{13,21-25} were obtained using different ways of generating the disorder. In this study, we consider the disorder generated by randomly choosing a fraction ρ_{pin} of the particles from an equilibrium configuration of the supercooled liquid at temperature T and freezing them in space. We henceforth refer to this geometry as the “random pinning” geometry. This kind of quenched disorder can be

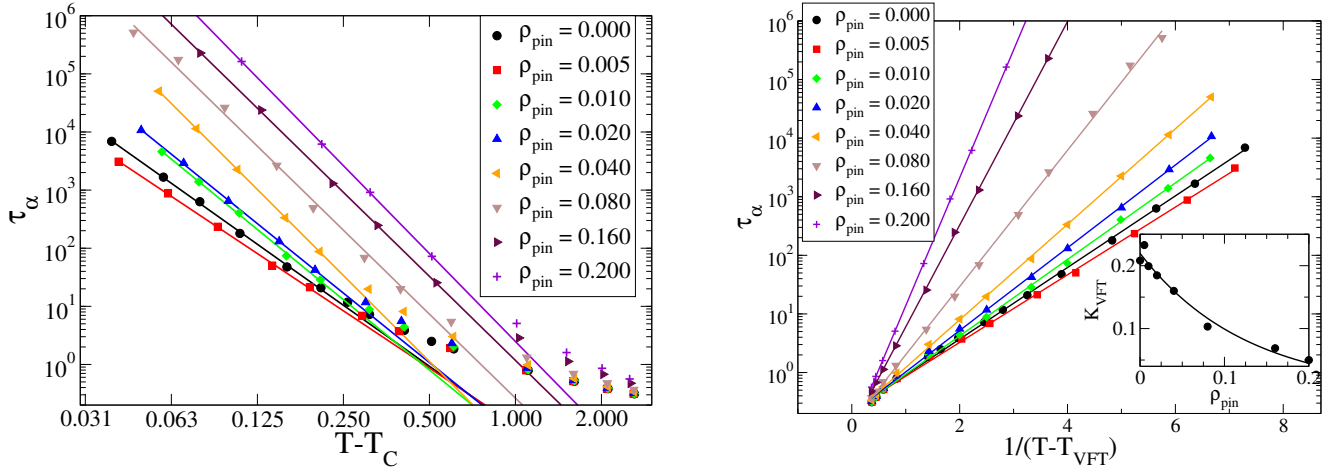


Figure 1. *Left Panel:* Power-law fits to obtain T_C as a function of ρ_{pin} for the 3dKA model. *Right Panel:* VFT fits to obtain T_{VFT} as a function of ρ_{pin} for the 3dKA model. *Inset:* Kinetic fragility K_{VFT} as a function of ρ_{pin} . The dramatic decrease in K_{VFT} with increasing ρ_{pin} can be clearly seen. The line is an exponential fit to the data.

realized in liquids confined in a statistically homogeneous porous medium²⁶ obtained by freezing a fraction of the particles in an equilibrium configuration of the same liquid. It can also be realized in experiments on colloidal systems,²⁰ using optical traps to pin the particles. This way of generating the disorder, considered in Ref.¹⁷ has certain advantages. For instance, preparing an equilibrated system is straightforward, as the state obtained by instantaneously freezing a randomly selected fraction of the particles in an equilibrated liquid configuration is a valid equilibrium configuration of the system with the pinning disorder. In earlier studies,^{13,22,24,25} the relaxation time of the system with random pinning was found to increase very rapidly with increasing concentration of the pinned particles. The RFOT description which forms the basis of the theoretical calculations of Ref.¹⁷ predicts a divergence of the structural relaxation time at the putative entropy-vanishing thermodynamic transition. Therefore, the phase diagram in the $(\rho_{pin} - T)$ plane can be obtained by locating the temperatures at which the relaxation time diverges for different values of the pin density. Since a rapid growth of the relaxation time is a defining feature of glassy behavior, the dynamics of pinned liquids is interesting by itself. For these reasons, we have carried out a detailed study of the dynamics for two model glass forming liquids in the presence of random pinning using extensive numerical simulations.

Theoretical predictions

Before going into the details of our results, we briefly discuss the arguments presented in Ref.¹⁷ about the phase diagram of the randomly pinned system in the $(\rho_{pin} - T)$ plane. In the RFOT theory, a thermodynamic glass transition is characterized by the vanishing of the configurational entropy density s_c associated with the multiplicity of amorphous local minima of the free energy. In Ref.¹⁷ the arguments of RFOT were extended to glass forming system with randomly pinned particles. It is physically reasonable to assume that the configurational entropy of a liquid decreases with increase pinning fraction ρ_{pin} . In Ref.¹⁷ it was assumed that the configurational entropy density decreases linearly with ρ_{pin} ,

$$s_c(T, \rho_{pin}) \simeq s_c(T, 0) - \rho_{pin}E(T), \quad (1)$$

for small values of ρ_{pin} , with $E(T) > 0$. In RFOT, $s_c(T, 0)$ is supposed to go to zero at the Kauzmann temperature $T_K(0)$, the argument of T_K being the value of ρ_{pin} . Eq.(1) then predicts that for $T > T_K(0)$, the configurational entropy should vanish at a critical pinning fraction $\rho_K(T) \simeq s_c(T, 0)/E(T)$ and a thermodynamic glass transition should occur at that pinning fraction. Assuming that this critical fraction $\rho_K(T) < 1$, the thermodynamic glass transition temperature $T_K(\rho_{pin})$, obtained from the condition $s_c(T_K, \rho_{pin}) = 0$, should increase from $T_K(0)$ as ρ_{pin} is increased from zero. In Ref.¹⁷ a MF analysis was carried out for the spherical p -spin model to calculate $T_K(\rho_{pin})$, as well as the critical temperature (T_C) of Mode Coupling Theory (MCT)²⁷ which represents the temperature below which the dynamics of the system is dominated by activated relaxation processes. It was shown that the dependence of these two temperatures, T_K and T_C , on ρ_{pin} are such that they meet at a ‘‘critical’’ value of ρ_{pin} , at which the thermodynamic glass transition disappears. A real-space RG calculation predicted that the line of thermodynamic glass transitions in the $(\rho_{pin} - T)$ plane has a positive slope and it ends at a critical value of ρ_{pin} . The dynamic transition at T_C is not found in the RG calculation.

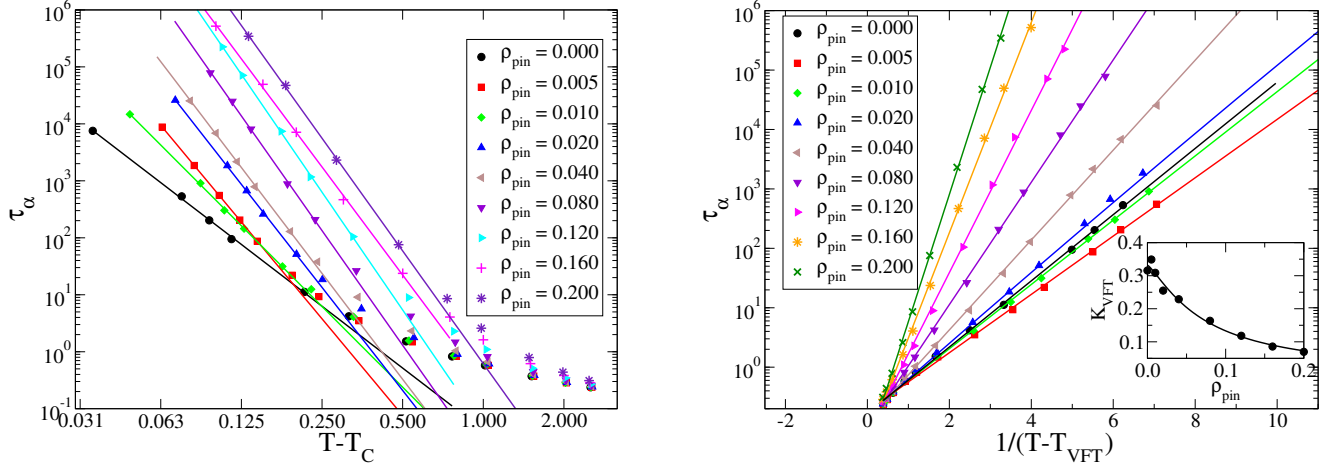


Figure 2. *Left Panel:* Power-law fits to obtain T_C as a function of ρ_{pin} for the 3dR10 model with $\gamma = 4$. *Right Panel:* VFT fits to obtain T_{VFT} as a function of ρ_{pin} for the 3dR10 model. *Inset:* Kinetic fragility K_{VFT} as a function of ρ_{pin} . The line corresponds to an exponential fit to the data.

Systems and Methods

The first model glass former we study is the well-known Kob-Andersen²⁸ 80 : 20 binary Lenard-Jones mixture. Here it will be referred to as the **3dKA model**. The temperature range studied for this model is $[0.45, 3.00]$ at number density $\rho = 1.20$. The second model studied is a 50 : 50 binary mixture with pairwise interactions between particles that fall off with distance as an inverse power-law with exponent 10 (the **3dR10 model**). The temperature range covered for this model is $[0.52, 3.00]$ at number density $\rho = 0.81$.

We performed NVT molecular dynamics simulations using modified leap-frog algorithm with the Berendsen thermostat. For both the model systems, we performed simulations for ρ_{pin} in the range $[0.000, 0.200]$ for each temperature. For very low temperatures, we were not able to equilibrate the system for high pin concentrations because of a dramatic increase in the relaxation time in these cases. (See SI for further details).

Dynamic properties are characterized by calculating the self part of a modified two-point density correlation function which we call the overlap correlation function $Q(t)$ defined as

$$Q(t) = \left\langle \frac{1}{N - N_{pin}} \sum_i' w(|\vec{r}_i(t) - \vec{r}_i(0)|) \right\rangle_0, \quad (2)$$

where the weight function $w(x) = 1.0$ if $x < 0.30$ and 0 otherwise, $\overline{\langle \dots \rangle}_0$ denotes averaging over the time origin and also averaging over different realizations of the disorder, and $N_{pin} = \rho_{pin}N$ is the number of pinned particles. The prime over the summation sign means that the sum is over only the unpinned particles. We average the data over 32 independent runs for each state point and consider systems with $N = 1000$. The α -relaxation time τ_α is calculated by the condition $Q(\tau_\alpha) = 1/e$. It is to be noted that τ_α -values obtained from the self intermediate scattering function $F_s(k, t)$, calculated at the wave-vector at which the static structure factor $S(k)$ peaks, are very close to those obtained using $Q(t)$.

We estimate the MCT crossover temperature T_C by fitting τ_α -values for different temperatures for a given value of ρ_{pin} to a power-law form, $\tau_\alpha \sim B/|T - T_C|^\gamma$ and the temperature T_{VFT} by fitting the data to a Vogel-Fulcher-Tammann law defined by $\tau_\alpha \sim \tau_\infty \exp[A/(T - T_{VFT})]$. It should be noted that earlier experimental and simulation studies have reported that $T_{VFT} \approx T_K$ for unpinned liquids. In the case of the power-law fit, for each value of ρ_{pin} , 4-5 data points with the highest values of τ_α were used for the fitting procedure. The kinetic fragility is obtained as $K_{VFT} = T_{VFT}/A$.

Results

Figures 1 and 2 show the MCT and VFT fits for the 3dKA and 3dR10 models respectively. One can clearly see that the VFT fits to the data for both the model systems are excellent, but the MCT fits are not very good over the whole temperature range. If a few data points at relatively high temperatures are excluded in the power-law fitting, a reasonable fit for low-temperature data points is obtained. This gives us confidence about the reliability of the extracted values of T_{VFT} and T_C , although both

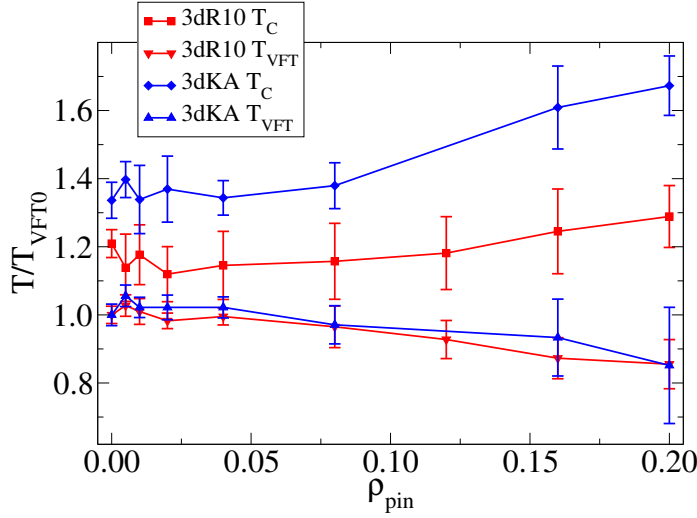
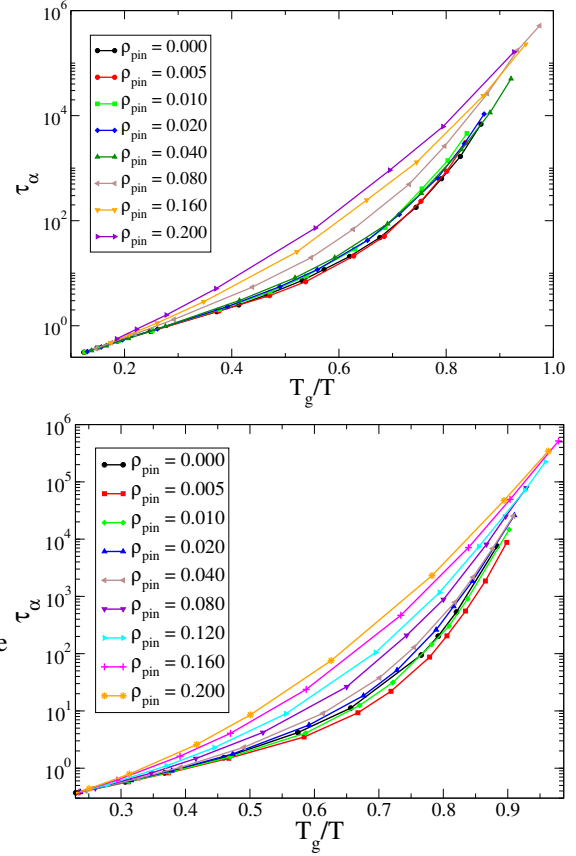


Figure 3. *Left panel:* Phase diagram – Variation of the MCT-transition temperature T_C and the VFT-divergence temperature T_{VFT} with ρ_{pin} for the 3dKA and the 3dR10 models. For comparison all temperatures are scaled by the VFT-divergence temperature for the unpinned system, T_{VFT0} . The lines join successive data points. *Top right panel:* Angell plots for the 3dKA model. *Bottom right panel:* Angell plots for the 3dR10 model.



estimations rely on extrapolation. This, however, is an unavoidable problem in studies of glassy dynamics, affecting both numerical and experimental investigations.

With these caveats, if the values of T_C and T_{VFT} extracted from the fits are used to construct a phase diagram in the $(\rho_{pin} - T)$ plane, one finds somewhat puzzling results as depicted in the left panel of Fig. 3. This figure shows the variation of T_{VFT} and T_C , scaled by the value of T_{VFT} for $\rho_{pin} = 0$, with ρ_{pin} . It is clear from the plots that T_C increases with increasing ρ_{pin} , as predicted in Ref.¹⁷ and in subsequent detailed MCT calculations.^{26,29} On the other hand, T_{VFT} does not show any indication of increasing with ρ_{pin} to meet the T_C line at a critical value of ρ_{pin} , as predicted in the MF analysis of Ref.¹⁷ Rather, it seems to remain constant or to decrease slowly as ρ_{pin} is increased. To cross-check these results, we have obtained the parameters of the VFT form from so-called “Stickel plots”.³⁰ We find that the values of T_{VFT} obtained from the lowest-temperature data points in the Stickel plots are close to those obtained from our VFT plots and exhibit very similar dependence on ρ_{pin} . The Stickel plots do not show any indication that this behavior will change at lower temperatures. The details of these results are provided in the SI. Another important and somewhat unexpected result of our study is that the kinetic fragility K_{VFT} decreases rapidly with increasing ρ_{pin} in both of our model systems. In the insets of Fig. 1 and Fig. 2, we have plotted K_{VFT} as a function of ρ_{pin} . One can see that this measure of fragility changes by a factor of 5 – 8 in the studied range of ρ_{pin} . To emphasize this point, we have constructed “Angell plots” in which the relaxation time is plotted as a function of the temperature scaled by T_g , defined as $\tau_\alpha(T_g) = 10^6$. These plots are also shown in Fig. 3. The dramatic change in the fragility, manifested as a change in the curvature of the plots, can be clearly seen in these Angell plots. Restricted fits in which K_{VFT} is fixed at the value for the unpinned liquid provide rather poor description of the data for relatively large values of ρ_{pin} (see the SI for details).

The phenomenological Adam-Gibbs relation,³¹ $\tau_\alpha(T) \propto \exp[B/(T s_c(T))]$, between the α -relaxation time and the configurational entropy density (B is a constant) leads to a VFT form for the temperature dependence of τ_α with $T_{VFT} = T_K$ if s_c behaves as $T s_c(T) = K(T - T_K)$ where K is a constant. Numerical results^{32,33} for the configurational entropy of liquids without pinning, obtained at relatively high temperatures at which the liquid can be equilibrated in time scales accessible in simulations, are consistent with this linear relation that extrapolates to zero at a temperature T_K that is close to the T_{VFT} obtained from a VFT fit to the temperature dependence of τ_α . If we assume that the Adam-Gibbs relation remains valid²⁵ in the presence of pinning and s_c actually goes to zero at $T = T_K = T_{VFT}$ (as in the RFOT theory), then a reduction in T_{VFT} with increasing ρ_{pin} would not be consistent with the physically reasonable expectation that $s_c(T, \rho_{pin})$ is a decreasing function of ρ_{pin} . However, our results are consistent, within error bars, with T_{VFT} being independent of ρ_{pin} . This can be reconciled with the requirement

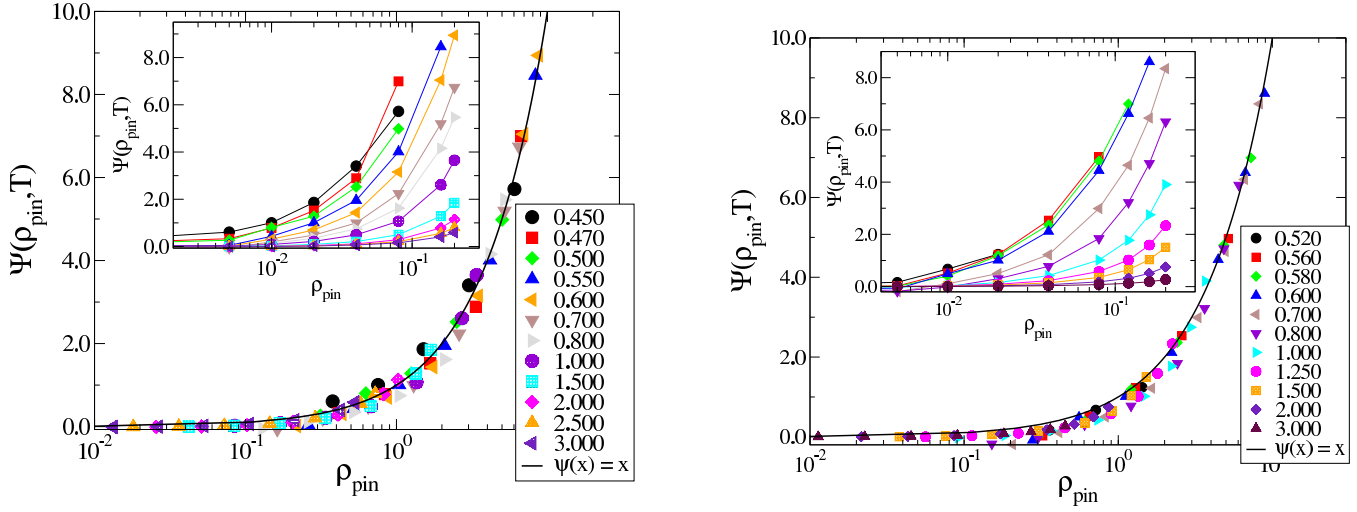


Figure 4. Data collapse using the scaling form in Eq. 9 to obtain the length-scale ξ_p . Left panel is for the 3dKA system and the right panel is for the 3dR10 system. In both cases, insets show the uncollapsed data.

of s_c decreasing with increasing ρ_{pin} if the dependence of s_c on T and ρ_{pin} is of the form

$$Ts_c(T, \rho_{pin}) = Ts_c(T, 0)F(T, \rho_{pin}) = K(T - T_{VFT})F(T, \rho_{pin}), \quad (3)$$

where $F(T, \rho_{pin})$, the fractional reduction of the configurational entropy due to pinning, decreases from 1 as ρ_{pin} is increased from 0. If the temperature dependence of $F(T, \rho_{pin})$ is weak (we ignore the dependence of F on T in the following discussion), then Eq.(3) and the Adam-Gibbs relation would lead to a VFT form for the temperature dependence of τ_α , with T_{VFT} independent of ρ_{pin} , in agreement with our observations. The fragility parameter $K_{VFT} = KT_{VFT}F(\rho_{pin})/B(\rho_{pin})$ would decrease with increasing ρ_{pin} (i.e. would agree with our observations) if F/B is a decreasing function of ρ_{pin} . We already know that F is a decreasing function of ρ_{pin} . The requirement that F/B be a decreasing function of ρ_{pin} would be satisfied if B increases, remains constant or decreases slower than F with increasing ρ_{pin} . In this scenario, the temperature dependence of τ_α for non-zero ρ_{pin} is given by

$$\tau_\alpha(\rho_{pin}, T) = \tau_\infty \exp \left[\frac{B(\rho_{pin})}{F(\rho_{pin})Ts_c(0, T)} \right]. \quad (4)$$

This implies the following relation between the relaxation times with and without pinning:

$$\ln \left[\frac{\tau_\alpha(\rho_{pin}, T)}{\tau_\alpha(0, T)} \right] = \frac{G(\rho_{pin})}{Ts_c(0, T)} \quad (5)$$

where the function $G(\rho_{pin})$ is defined by

$$G(\rho_{pin}) \equiv B(\rho_{pin})/F(\rho_{pin}) - B(0)/F(0). \quad (6)$$

It is clear from the definition that $G(0) = 0$ and assuming that G and F are smooth functions of ρ_{pin} , we get

$$G(\rho) = C\rho_{pin} + \dots \quad (7)$$

where C is a constant and \dots represent terms with higher powers of ρ_{pin} , which can be neglected for small values of ρ_{pin} . So, for small values of ρ_{pin} , Eq.(5) becomes

$$\ln \left[\frac{\tau_\alpha(\rho_{pin}, T)}{\tau_\alpha(0, T)} \right] = \frac{C\rho_{pin}}{Ts_c(0, T)} \quad (8)$$

which has the form of a scaling relation,

$$\ln \left[\frac{\tau_\alpha(\rho_{pin}, T)}{\tau_\alpha(0, T)} \right] = Cf(\rho_{pin}\xi_p^d(T)) \quad (9)$$

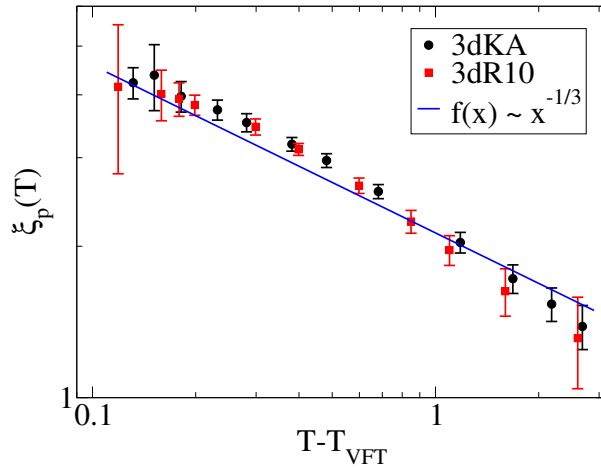


Figure 5. Pinning length scale ξ_p as a function of temperature T .

with $f(x) = x$ and the pinning length scale ξ_p given by $\xi_p(T) = [1/(T s_c(0, T))]^{1/d} \propto [1/(T - T_{VFT})]^{1/d}$ (d is the spatial dimension).

To test this scaling prediction, we have tried to collapse the data for $\psi(\rho_{pin}, T) \equiv \ln[\tau_\alpha(\rho_{pin}, T)/\tau_\alpha(0, T)]$ for all temperatures and pinning densities into a single scaling curve by choosing the length scale $\xi_p(T)$ appropriately for different temperatures. As shown in Fig. 4, good data collapse is obtained for both the model systems studied. The line passing through the collapsed data is indeed of the form predicted by the scaling argument. We have also checked whether the $\xi_p(T)$ obtained from the scaling collapse is proportional to $[1/(T - T_{VFT})]^{1/d}$. In Fig. 5, we have plotted the pinning length scale ξ_p as a function of $(T - T_{VFT})$ for both the model systems. The results are clearly consistent with the scaling argument. It is interesting to note that although our results for the phase diagram do not agree with the prediction of Ref.,¹⁷ the temperature dependence of the pinning length $\xi_p(T)$ turns out to be the same as that in Ref.¹⁷

It is also possible that $F(\rho_{pin})$ goes to zero at a value of ρ_{pin} higher than the largest value considered in our simulations. If this happens, then the line of (putative) thermodynamic glass transitions in the $(T - \rho_{pin})$ plane would end at this “critical” value of ρ_{pin} . This would be similar to the phase diagram obtained in the RG calculation reported in Ref.¹⁷ with the important difference that the transition line would be parallel to the ρ_{pin} axis. It should, however, be noted that the arguments above do not depend on the assumption that a thermodynamic glass transition arising from the vanishing of s_c actually occurs in liquids without pinning. Since numerically obtained values of $s_c(T, 0)$ at the relatively high temperatures considered in our simulations satisfy the relation $T s_c(T, 0) = K(T - T_{VFT})$ irrespective of whether s_c actually goes to zero at a non-zero temperature, our results are also compatible with scenarios, such as those based on the behavior of kinetically constrained models,¹⁸ in which a thermodynamic glass transition does not occur at any non-zero temperature. In such a scenario, a slow reduction of the value of T_{VFT} , obtained from fitting the simulation data for τ_α to the VFT form, with increasing pin concentration would not be incompatible with the physical requirement of s_c decreasing with increasing ρ_{pin} .

Comparison with Other Numerical Results

Our results for the phase diagram in the $(\rho_{pin} - T)$ plane, with T_{VFT} identified with T_K , are in disagreement with those of two recent numerical studies.^{24,34} In Ref.,²⁴ the dependence of T_K on ρ_{pin} was obtained from simulations of a 64-particle system of harmonic spheres. The temperature T_K , obtained from the behavior of the distribution of an overlap parameter similar to that defined in Eq.(2), was found to increase with increasing ρ_{pin} . We believe that the results reported in Ref.²⁴ suffer from strong finite-size effects. As shown in that paper, the basic form of the distribution (whether it is unimodal or bimodal) for a system with 64 particles can be different from that for a system with 128 particles. Similar results for strong finite-size effects in the distribution of a similar overlap parameter were reported earlier.¹² Since a change in the distribution from unimodal to bimodal is supposed to signal the transition from the liquid to the glass phase, the data for the distribution obtained for a system with 64 particles cannot provide reliable quantitative information about the location of the transition point in the $(\rho_{pin} - T)$ plane. This, we believe, is the primary reason for the difference between our results and those of Ref.²⁴ We have also found that the fragility for a 64-particle system (3dR10 model) is substantially smaller than that for a system with 1000 particles. Since our results show that the main effect of pinning is a reduction of the fragility, studies of small systems in which the fragility is strongly affected by system size are not expected to provide a reliable description of the effects of pinning. In another recent study,³⁴ the configurational entropy density s_c of the 3dKA model was calculated for different pin densities and temperatures and the

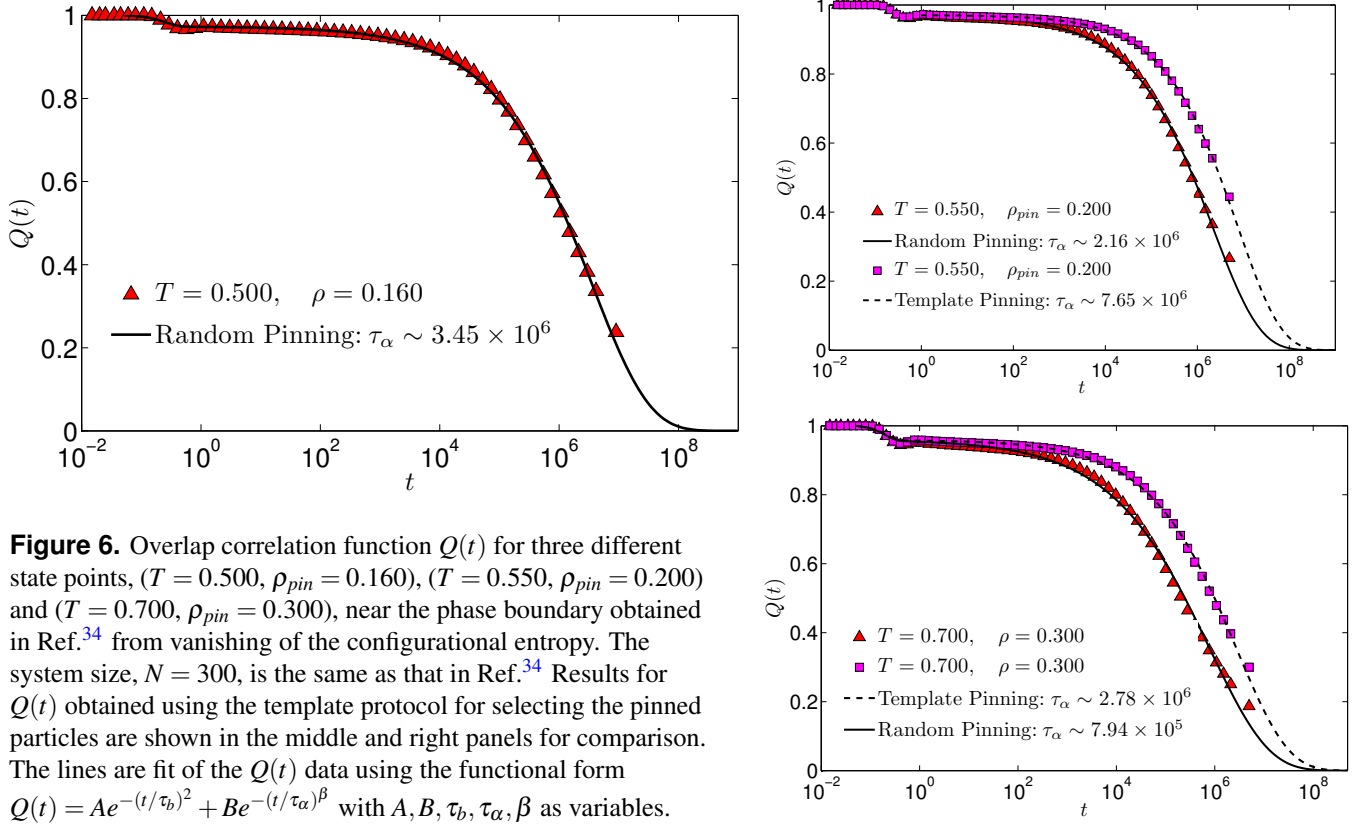


Figure 6. Overlap correlation function $Q(t)$ for three different state points, $(T = 0.500, \rho_{pin} = 0.160)$, $(T = 0.550, \rho_{pin} = 0.200)$ and $(T = 0.700, \rho_{pin} = 0.300)$, near the phase boundary obtained in Ref.³⁴ from vanishing of the configurational entropy. The system size, $N = 300$, is the same as that in Ref.³⁴ Results for $Q(t)$ obtained using the template protocol for selecting the pinned particles are shown in the middle and right panels for comparison. The lines are fit of the $Q(t)$ data using the functional form $Q(t) = Ae^{-(t/\tau_b)^2} + Be^{-(t/\tau_\alpha)^\beta}$ with $A, B, \tau_b, \tau_\alpha, \beta$ as variables.

phase boundary in the $(\rho_{pin} - T)$ plane was obtained by estimating the values of ρ_{pin} at which s_c goes to zero for different temperatures. The value of T_K obtained in this way was found to increase with increasing pin concentration. These results, obtained from the behavior of thermodynamic quantities, are quite different from those obtained in our work from the dynamics of the system.

To resolve this discrepancy, we have simulated the dynamics of the 3dKA model at a few points in the $(\rho_{pin} - T)$ plane at which s_c is supposed to go to zero according to the phase diagram obtained in Ref.³⁴ In these simulations, we considered the same system size ($N = 300$) as that in Ref.³⁴ to remove any ambiguity that may arise from finite-size effects (we found similar results for $N = 1000$, indicating that finite-size effects for the dynamics are weak for systems with 300 or more particles). Surprisingly, we found that it is possible to equilibrate the system in time scales accessible in MD simulations at the points where s_c is supposed to go to zero or to have a very small value. Results for the overlap function $Q(t)$ at three “transition points”, $(T = 0.50, \rho_{pin} = 0.16)$, $(T = 0.55, \rho_{pin} = 0.20)$ and $(T = 0.70, \rho_{pin} = 0.30)$, are shown in Fig. 6. The relaxation times at these points are estimated to be of the order of $10^6 - 10^7$, as indicated in the legends of the respective plots. This is very different from the behavior of systems without pinning, for which it is impossible to equilibrate the system in time scales accessible in MD simulations at temperatures close to the value at which s_c is supposed to go to zero. For example, τ_α in the unpinned 3dKA model attains the value of 10^7 at a temperature that is 25% higher than the temperature at which s_c extrapolates to zero.

These results seem to imply that the relaxation time is *finite* at points in the $(\rho_{pin} - T)$ plane where s_c goes to zero (or has a very small value) according to the results reported in Ref.³⁴ While the possibility that the relaxation time does not diverge when the configurational entropy vanishes cannot be ruled out, we believe that this is unlikely to be the explanation of the seemingly contradictory results mentioned above. The dependence of τ_α on s_c may not be the Adam-Gibbs relation (it is suggested in Ref.³⁴ that the Adam-Gibbs relation is violated in pinned systems), but a violation of the physically reasonable expectation that τ_α should diverge if s_c goes to zero would be quite surprising. A more probable explanation of these results is that s_c does not actually go to zero at the phase boundary obtained in Ref.³⁴ The calculation of s_c in Ref.³⁴ requires estimation of the “basin entropy” which is calculated using a harmonic approximation. Anharmonic effects at the relatively high temperatures considered for pinned systems may cause inaccuracies in the estimation of s_c , leading to errors in the determination of the phase boundary in the $(\rho_{pin} - T)$ plane. One of the signatures of this effect has been pointed out by the authors of Ref.³⁴ as the negative values of the configurational entropy at some state points. Another point to note is that the pinned particles were chosen randomly in our simulations, whereas a “template” method was used in Ref.³⁴ We have found that time scales obtained for template pinning are systematically larger than those for randomly pinned systems at the same temperature and pin density.

Typical results for ($T = 0.55$, $\rho_{pin} = 0.20$) and ($T = 0.70$, $\rho_{pin} = 0.30$) are shown in the middle and right panels of Fig. 6. It is not clear whether this difference between the protocols used for selecting the pinned particles would account for the difference between our results and those of Ref.³⁴ It would be interesting to find out whether the configurational entropy is affected by the choice of the protocol. It is argued in Ref.³⁴ that template pinning reduces sample-to-sample fluctuations compared to random pinning, but we found that fluctuations in the overlap function are of similar magnitude for both protocols. It is also possible (but very unlikely) that the plots for $Q(t)$ in Fig. 6 would level off at time scales longer than those considered in our simulations, leading to very large values of the relaxation time. The excellent fits of the data for $Q(t)$ to a stretched exponential form, shown in Fig. 6, strongly argues against this possibility.

In a recent numerical study³⁵ of the dynamics of the Kob-Andersen mixture in the presence of random pinning of the kind considered here, it was found, from VFT fits to the data for τ_α as a function of ρ_{pin} at a fixed temperature T , that the values of ρ_{pin} at which τ_α appears to diverge are large ($\simeq 0.58$) and essentially independent of T for $T \leq 0.7$. These ‘‘critical’’ values of ρ_{pin} are very different from those predicted in the phase diagram of Ref.³⁴ The dynamic behavior found in Ref.³⁵ is qualitatively similar to that found in our study and consistent with the behavior of the configurational entropy proposed in Eq.(3) with $F(\rho_{pin})$ going to zero at $\rho_{pin} \simeq 0.58$.

Conclusion

In summary, we have obtained the phase diagram of two model glass forming liquids with randomly pinned particles from a study of the temperature dependence of the structural relaxation time and found that the MCT temperature T_C increases, in agreement with the predictions of Ref.,¹⁷ whereas the VFT-divergence temperature T_{VFT} remains nearly constant or decreases slowly with increasing pin concentration. The second observation is important because it is in disagreement with the predictions of Refs.^{17,24,34} if we assume (as is done in the RFOT description) that a thermodynamic transition at which the configurational entropy density s_c goes to zero coincides with a divergence of the relaxation time. If we interpret our results as indicating that T_{VFT} decreases with increasing pin concentration, then the unavoidable conclusion would be that the thermodynamic glass transition of RFOT *does not* take place in these systems. An interpretation of our results as showing that T_{VFT} is independent of the pin concentration would imply that (a) the RG calculation of Ref.¹⁷ is not quantitatively accurate and that (b) the dependence of T_{VFT} on ρ_{pin} found in Refs.²⁴ and³⁴ is not quantitatively accurate. In either case, the original expectation that the addition of quenched random pinning would make the thermodynamic glass transition accessible to experiments and simulations would not be fulfilled. It is also possible (though unlikely in our opinion) that a vanishing of s_c does not correspond to a divergence of τ_α in the pinned systems considered here. This would imply that the RFOT description does not apply to these systems.

These findings will help in interpreting the results of experiments²⁰ on colloidal systems with random pinning. We also find a rapid reduction of the kinetic fragility with increasing pin concentration. Our results indicate that a reduction of the fragility, rather than an increase in the VFT-divergence temperature, is responsible for the increase in the relaxation time with increasing pin concentration. Since the fragility changes by factor of 5 – 8 as the pin concentration is changed, model liquids with randomly pinned particles may also be useful for understanding the role of fragility in the glass transition.

Acknowledgments

We would like to thank Srikanth Sastry for useful discussions. S.C. wishes to thank the UGC’s Dr. D.S. Kothari Fellowship for financial support and TCIS for hospitality.

Author contributions statement

S.C. and S.K. performed simulations and analyzed data. S.K and C.D. guided the research and provided the main ideas. All authors wrote the manuscript.

References

1. Cavagna, A. Supercooled liquids for pedestrians. *Phys. Rep.* **476**, 51–124 (2009).
2. Berthier, L. & Biroli, G. Theoretical perspective on the glass transition and amorphous materials. *Rev. Mod. Phys.* **83**, 587–645 (2011).
3. Kirkpatrick, T. R., Thirumalai, D. & Wolynes, P. G. Scaling concepts for the dynamics of viscous liquids near an ideal glassy state. *Phys. Rev. A* **40**, 1045–1054 (1989).
4. Lubchenko, V. & Wolynes, P. G. Theory of structural glasses and supercooled liquids. *Annu. Rev. Phys. Chem.* **58**, 235–266 (2007).

5. Biroli, G. & Bouchaud, J.-P. The random first-order transition theory of glasses: a critical assessment. *Structural Glasses and Supercooled Liquids: Theory, Experiment, and Applications* 31–113 (2012).
6. Chandler, D. & Garrahan, J. P. Dynamics on the way to forming glass: Bubbles in space-time. *Ann. Rev. Phys. Chem.* **61**, 191–217 (2007).
7. Karmakar, S., Dasgupta, C. & Sastry, S. Growing length scales and their relation to timescales in glass-forming liquids. *Annu. Rev. Condens. Matter Phys.* **5**, 255–284 (2014).
8. Ediger, M. D. Spatially heterogeneous dynamics in supercooled liquids. *Annu. Rev. Phys. Chem.* **51**, 99–128 (2000).
9. Berthier, L. *et al.* Direct experimental evidence of a growing length scale accompanying the glass transition. *Science* **310**, 1797–1800 (2005).
10. Biroli, G., Bouchaud, J.-P., Miyazaki, K. & Reichman, D. R. Inhomogeneous mode-coupling theory and growing dynamic length in supercooled liquids. *Phys. Rev. Lett.* **97**, 195701 (2006).
11. Biroli, G., Bouchaud, J.-P., Cavagna, A., Grigera, T. S. & Verrocchio, P. Thermodynamic signature of growing amorphous order in glass-forming liquids. *Nat. Phys.* **4**, 771–775 (2008).
12. Karmakar, S., Dasgupta, C. & Sastry, S. Growing length and time scales in glass-forming liquids. *Proc. Nat'l Acad. Sci. USA* **106**, 3675–3679 (2009).
13. Karmakar, S., Lerner, E. & Procaccia, I. Direct estimate of the static length-scale accompanying the glass transition. *Physica A: Statistical Mechanics and its Applications* **391**, 1001–1008 (2012).
14. Hocky, G. M., Markland, T. E. & Reichman, D. R. Growing point-to-set length scale correlates with growing relaxation times in model supercooled liquids. *Phys. Rev. Lett.* **108**, 225506 (2012).
15. Karmakar, S. & Procaccia, I. Finite-size scaling for the glass transition: The role of a static length scale. *Phys. Rev. E* **86**, 061502 (2012).
16. Biroli, G., Karmakar, S. & Procaccia, I. Comparison of static length scales characterizing the glass transition. *Phys. Rev. Lett.* **111**, 165701 (2013).
17. Cammarota, C. & Biroli, G. Ideal glass transitions by random pinning. *Proc. Nat'l Acad. Sci. USA* **109**, 8850–8855 (2012).
18. Garrahan, J. P., Sollich, P. & Toninelli, C. Kinetically constrained models. *Dynamical heterogeneities in Glasses, colloids and granular media and jamming transitions, International series of monographs in physics (Oxford University Press, Oxford, 2011) Chap 10*, 341–369 (2011).
19. Jack, R. L. & Berthier, L. Random pinning in glassy spin models with plaquette interactions. *Phys. Rev. E* **85**, 021120 (2012).
20. Gokhale, S., Nagamanasa, K. H., Ganapathy, R. & Sood, A. Growing dynamical facilitation on approaching the random pinning colloidal glass transition. *Nature communications* **5** (2014).
21. Karmakar, S. & Parisi, G. Random pinning glass model. *Proc. Nat'l Acad. Sci. USA* **110**, 2752–2757 (2013).
22. Kim, K. Effects of pinned particles on the structural relaxation of supercooled liquids. *Europhys. Lett.* **61**, 790 (2003).
23. Berthier, L. & Kob, W. Static point-to-set correlations in glass-forming liquids. *Phys. Rev. E* **85**, 011102 (2012).
24. Kob, W. & Berthier, L. Probing a liquid to glass transition in equilibrium. *Phys. Rev. Lett.* **110**, 245702 (2013).
25. Kob, W. & Coslovich, D. Nonlinear dynamic response of glass-forming liquids to random pinning. *Phys. Rev. E* **90**, 052305 (2014).
26. Krakoviack, V. Mode-coupling theory predictions for the dynamical transitions of partly pinned fluid systems. *Phys. Rev. E* **84**, 050501 (2011).
27. Das, S. P. Mode-coupling theory and the glass transition in supercooled liquids. *Reviews of modern physics* **76**, 785 (2004).
28. Kob, W. & Andersen, H. C. Testing mode-coupling theory for a supercooled binary Lennard-Jones mixture I: The van Hove correlation function. *Phys. Rev. E* **51**, 4626–4641 (1995).
29. Szamel, G. & Flenner, E. Glassy dynamics of partially pinned fluids: An alternative mode-coupling approach. *Europhys. Lett.* **101**, 66005 (2013).
30. Stickel, F., Fischer, E. & Richert, R. Dynamics of glass-forming liquids. i. temperature-derivative analysis of dielectric relaxation data. *J. Chem. Phys.* **102**, 6251–6257 (1995).

31. Adam, G. & Gibbs, J. H. On the temperature dependence of cooperative relaxation properties in glass-forming liquids. *J. Chem. Phys.* **43**, 139–146 (1965).
32. Sengupta, S., Karmakar, S., Dasgupta, C. & Sastry, S. Adam-gibbs relation for glass-forming liquids in two, three, and four dimensions. *Phys. Rev. Lett.* **109**, 095705 (2012).
33. Sengupta, S., Vasconcelos, F., Affouard, F. & Sastry, S. Dependence of the fragility of a glass former on the softness of interparticle interactions. *J. Chem. Phys.* **135**, 194503 (2011).
34. Ozawa, M., Kob, W., Ikeda, A. & Miyazaki, K. Equilibrium phase diagram of a randomly pinned glass-former. *arXiv:1412.4911* (2014).
35. Li, Yan-Wei, Zhu, You-Liang, & Sun, Zhao-Yan Decoupling of relaxation and diffusion in random pinning glass-forming liquids. *J. Chem. Phys.* **142**, 124507 (2015).

Phase Diagram of Glass Forming Liquids with Randomly Pinned Particles – Supplementary Information

Saurish Chakrabarty¹, Smarajit Karmakar², and Chandan Dasgupta^{1,3}

¹ Centre for Condensed Matter Theory, Department of Physics,
Indian Institute of Science, Bangalore, 560012, India,

² Centre for Interdisciplinary Sciences, Tata Institute of Fundamental Research,
21 Brundavan Colony, Narasingi, Hyderabad, India,

³ Jawaharlal Nehru Centre for Advanced Scientific Research, Bangalore 560064, India.

I. MODEL AND SIMULATION

The first model glass former we study is the well-known Kob-Andersen [1] 80 : 20 binary Lennard-Jones mixture. In the main article it is referred to as the 3dKA model. The interaction potential in this model is given by

$$V_{\alpha\beta}(r) = 4\epsilon_{\alpha\beta} \left[\left(\frac{\sigma_{\alpha\beta}}{r} \right)^{12} - \left(\frac{\sigma_{\alpha\beta}}{r} \right)^6 \right], \quad (1)$$

where $\alpha, \beta \in \{A, B\}$ and $\epsilon_{AA} = 1.0$, $\epsilon_{AB} = 1.5$, $\epsilon_{BB} = 0.5$, $\sigma_{AA} = 1.0$, $\sigma_{AB} = 0.80$, $\sigma_{BB} = 0.88$. The interaction potential is cut off at $2.50\sigma_{\alpha\beta}$ and we use a quadratic polynomial to make the potential and its first two derivatives smooth at the cutoff distance. The temperature range studied for this model is $T \in \{0.450, 3.000\}$ at number density $\rho = 1.20$. The second model studied is a 50 : 50 binary mixture with pairwise interactions between the particles that falls off with distance as an inverse power law as

$$V_{\alpha\beta}(r) = \epsilon_{\alpha\beta} \left(\frac{\sigma_{\alpha\beta}}{r} \right)^n, \quad (2)$$

with exponent $n = 10$ (the 3dR10 model). The potential is cut off at $1.38\sigma_{\alpha\beta}$. We again use a quadratic polynomial to make the potential and its first two derivatives smooth at the cutoff. The parameters of the potential are: $\epsilon_{\alpha\beta} = 1.0$, $\sigma_{AA} = 1.0$, $\sigma_{AB} = 1.22$ and $\sigma_{BB} = 1.40$. The temperature range covered for this model is $T \in \{0.52, 3.00\}$ at number density $\rho = 0.81$.

NVT molecular dynamics simulations are done in a cubic simulation box with periodic boundary conditions in three dimensions for both the model systems. We use the modified leap-frog algorithm with the Berendsen thermostat to keep the temperature constant in the simulation runs. Length, energy and time scales are measured in units of σ_{AA} , ϵ_{AA} and $\sqrt{\sigma_{AA}^2/\epsilon_{AA}}$. The integration time step used is $dt = 0.005$ in this temperature range. Equilibration runs are performed for $\sim 10^8 - 10^9$ MD steps depending on the temperature and production runs are long enough to ensure that the two-point density correlation function $Q(t)$ goes to zero within the simulation time. For both the model systems, we have performed simulations for pin concentration in the range $\rho_{pin} \in \{0.005, 0.200\}$ for each temperature. For very low temperatures, we were not able to equilibrate the system for high pin concentrations because of a dramatic increase in the relaxation time in these cases.

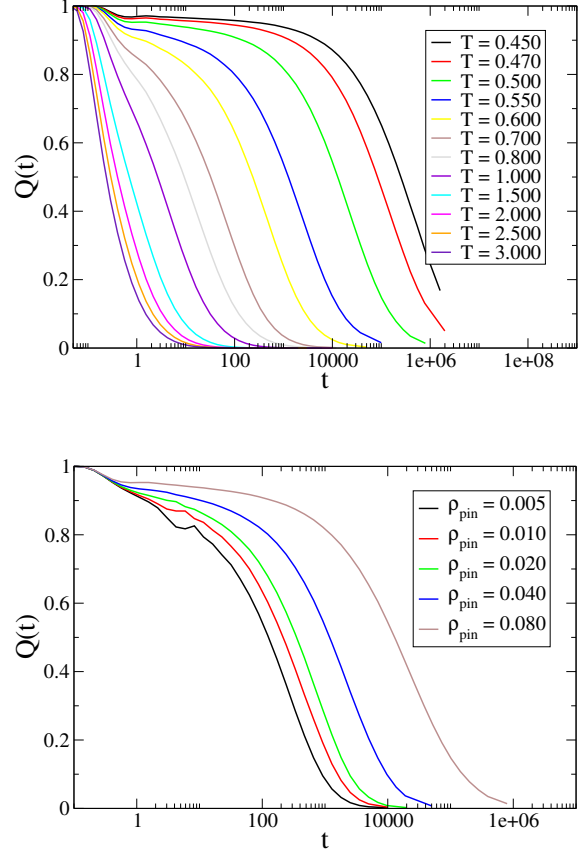


FIG. 1: *Top Panel:* $Q(t)$ for $\rho_{pin} = 0.080$ for various temperatures for the 3dKA model. *Bottom Panel:* $Q(t)$ for $T = 0.500$ for various levels of pinning for the 3dKA model.

II. TYPICAL OVERLAP CORRELATION FUNCTIONS

Some typical overlap correlation functions $Q(t)$, from our simulations have been plotted in Figs. 1 and 2. The set has data covering the entire range of relaxation times we obtained. The relaxation time τ_α was calculated using $Q(\tau_\alpha) = \exp(-1)$.

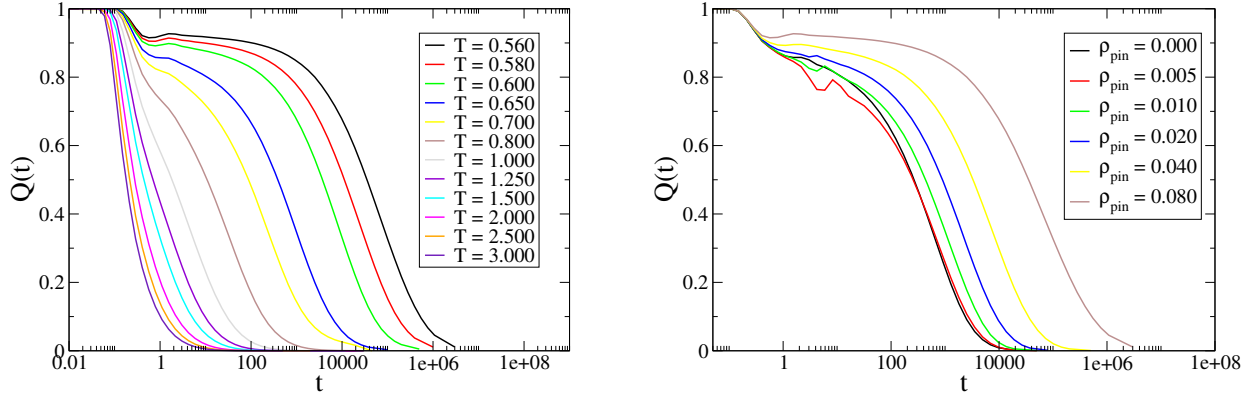


FIG. 2: *Left Panel:* $Q(t)$ for $\rho_{pin} = 0.080$ for various temperatures for the $3dR10$ model. *Right Panel:* $Q(t)$ for $T = 0.560$ for various levels of pinning for the $3dR10$ model.

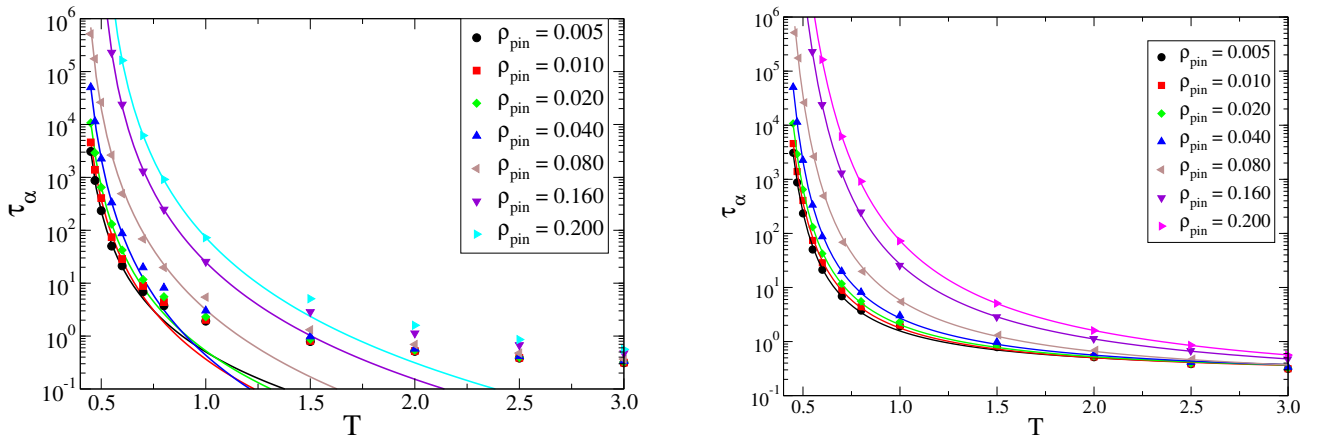


FIG. 3: *Left Panel:* Power law fit to obtain T_C as a function of ρ_{pin} for the $3dKA$ model. *Right Panel:* VFT fit to obtain T_K as a function of ρ_{pin} for the $3dKA$ model.

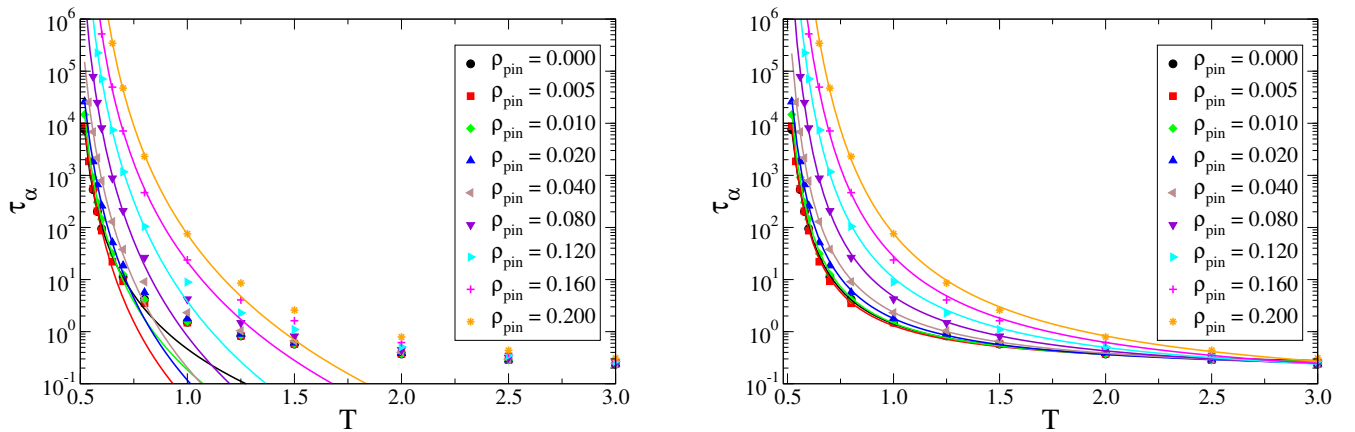


FIG. 4: *Left Panel:* Power law fit to obtain T_C as a function of ρ_{pin} for the $3dR10$ model. *Right Panel:* VFT fit to obtain T_K as a function of ρ_{pin} for the $3dR10$ model.

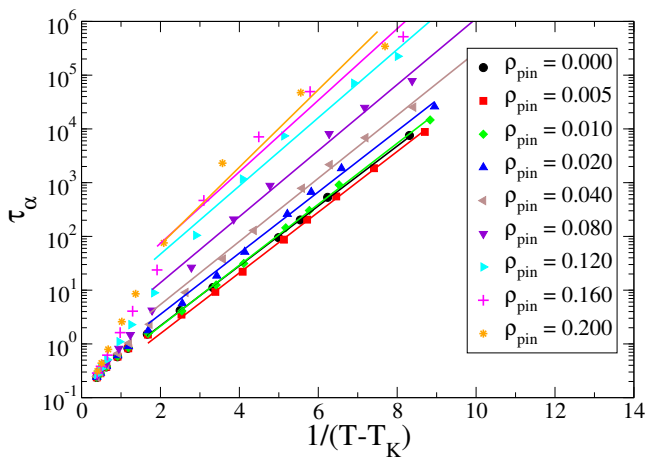
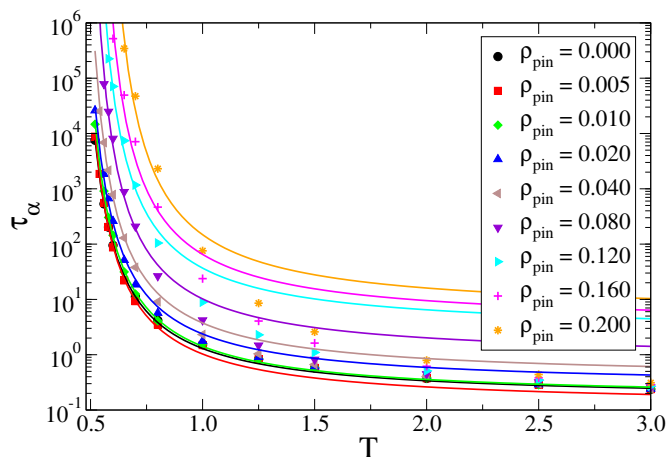
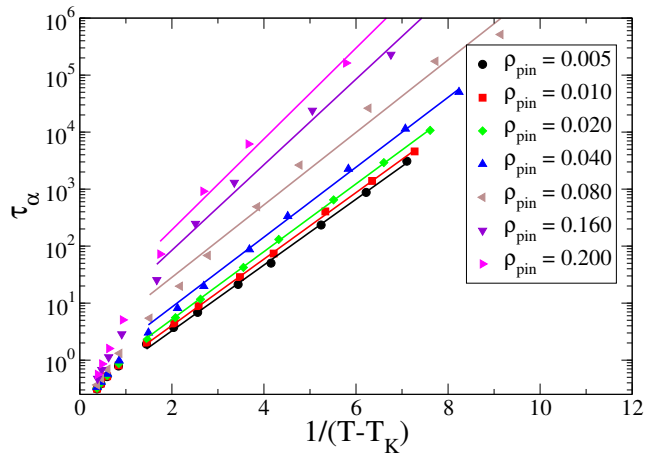
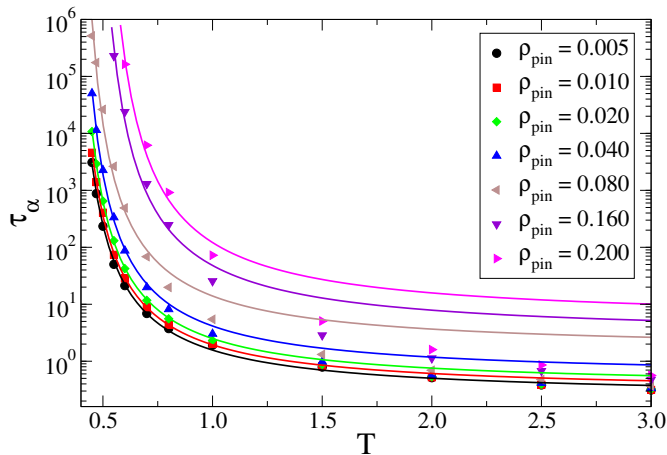


FIG. 5: *Left Panel*: VFT fit with fixed fragility for the $3dKA$ model. *Right Panel*: VFT fit with fixed fragility for the $3dR10$ model.

FIG. 6: *Left Panel*: Straight line plots for the VFT fit with fixed fragility for the $3dKA$ model. *Right Panel*: Straight line plots for the VFT fit with fixed fragility for the $3dR10$ model.

III. FITTING PROCEDURE

The fitting was done using the method of least squares. The natural logarithm of the relaxation time, $\ln(\tau_\alpha)$ was calculated first and the fitting was done using the $\ln(\tau_\alpha)$ versus T data. The error bars for the parameters obtained from the fit were calculated from the error in the τ_α -data using the following procedure. For each value of τ_α , we generated uniformly distributed data lying within the full width at half maximum of a Gaussian distribution with mean τ_α and variance $(\delta\tau_\alpha)^2$ ($\delta\tau_\alpha$ being the error in τ_α). Fits were done to 100 independent sets of such data. The spread in the parameters obtained from these fits were taken as the errors in the fit parameters.

The power-law and VFT fits for the two studied models are shown in Figs. 3 and 4. The same has been presented in the main paper in a way so that the fits appear as straight lines. The T_K and T_C values obtained from the fits are plotted in Tables I and II.

ρ_{pin}	T_K	T_C
0.000	0.4012 ± 0.0102	0.4852 ± 0.0165
0.005	0.4122 ± 0.0126	0.4567 ± 0.0396
0.010	0.4052 ± 0.0152	0.4721 ± 0.0352
0.020	0.3942 ± 0.0092	0.4492 ± 0.0324
0.040	0.3992 ± 0.0099	0.4595 ± 0.0401
0.080	0.3872 ± 0.0246	0.4643 ± 0.0447
0.120	0.3722 ± 0.0225	0.4740 ± 0.0429
0.160	0.3502 ± 0.0242	0.4996 ± 0.0499
0.200	0.3432 ± 0.0289	0.5171 ± 0.0365

TABLE I: T_K and T_C values obtained from the VFT and MCT fits at various levels of pinning for the $3dR10$ model.

ρ_{pin}	T_K	T_C
0.005	0.3092 ± 0.0098	0.4092 ± 0.0163
0.010	0.2993 ± 0.0092	0.3921 ± 0.0310
0.020	0.2993 ± 0.0112	0.4010 ± 0.0300
0.040	0.2993 ± 0.0095	0.3935 ± 0.0157
0.080	0.2843 ± 0.0173	0.4039 ± 0.0208
0.160	0.2733 ± 0.0349	0.4712 ± 0.0377
0.200	0.2494 ± 0.0528	0.4899 ± 0.0270

TABLE II: T_K and T_C values obtained from the VFT and MCT fits at various levels of pinning for the 3dKA model.

A. Power law divergence

The form assumed was

$$\tau_\alpha = \frac{A}{(T - T_C)^\gamma}, \quad (3)$$

where A is a constant pre-factor having appropriate dimensions, γ is the exponent for the divergence, and T_C is the (putative) transition temperature of mode coupling theory. For each value of the pinning density ρ_{pin} , 4-5 data points with the highest values of τ_α were used for the fitting procedure.

B. VFT divergence

The form assumed was

$$\tau_\alpha = \tau_\infty \exp \left[\frac{1}{K_{VFT} \left(\frac{T}{T_K} - 1 \right)} \right], \quad (4)$$

where τ_∞ is the high temperature relaxation time, K_{VFT} is the kinetic fragility and T_K is the Kauzmann temperature.

1. Fixed fragility

We obtained the same VFT fits also with fixed fragility. These are shown in Figs. 5 and 6. Since the fragility does not change with pinning density, these fits were good only in the low temperature regime. As such, for these fits, we only used those data points for which $\tau_\alpha > 10$. The phase diagram obtained using these fits is shown in the left panel of Fig. 7.

C. Onset temperature

The onset of super-Arrhenius behavior is marked by the temperature T_{onset} . This has been estimated by observing the meeting of the Arrhenius fit to the high temperature data and the super-Arrhenius fit to the low temperature data. This meeting point marks the crossover

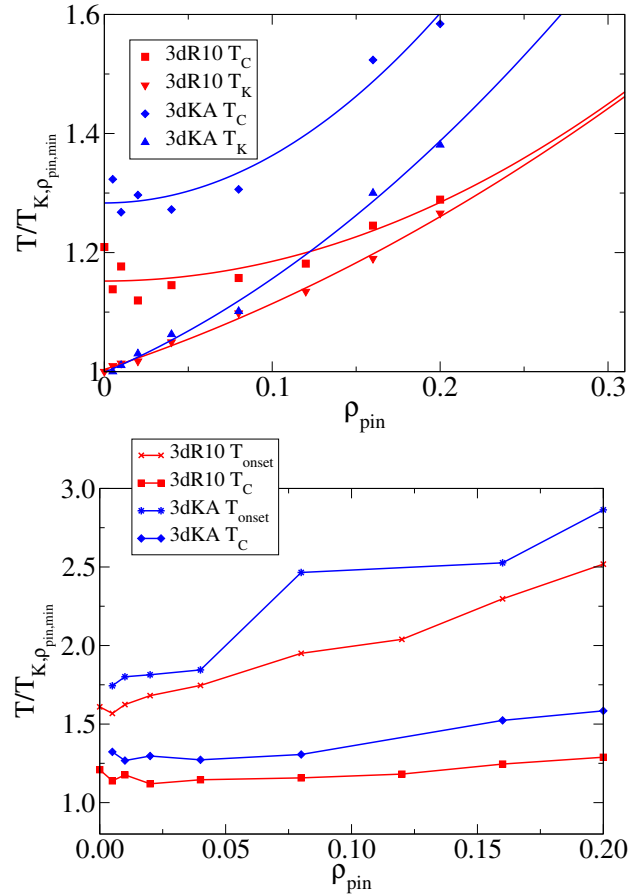


FIG. 7: *Left Panel:* The phase diagram with values of T_K obtained from fits with a fixed value of the kinetic fragility. The lines are quadratic fits to the data. The fits for the T_C data were done without a linear term. *Right Panel:* Variation of the MCT-transition temperature T_C and the onset temperature T_{onset} with ρ_{pin} for the 3dKA and the 3dR10 models.

from the high temperature Arrhenius behavior to the low temperature super-Arrhenius behavior. The predictions based on MF and RFOT analysis suggest that T_{onset} should approach T_C as ρ_{pin} is increased [2]. Our results, plotted in the right panel of Fig. 7, do not support this prediction.

D. Stickel Plots

An efficient way to verify the validity of the VFT form for the divergence of the relaxation time at T_K was introduced in Ref. [3]. This method involves analyses of the derivative of the viscosity (or α relaxation time) with respect to the temperature. A quantity $\Phi(T)$ is calculated using the data for the relaxation times as follows.

$$\Phi(T) \equiv \left(\frac{d \ln \tau_\alpha}{d(1/T)} \right)^{-\frac{1}{2}}. \quad (5)$$

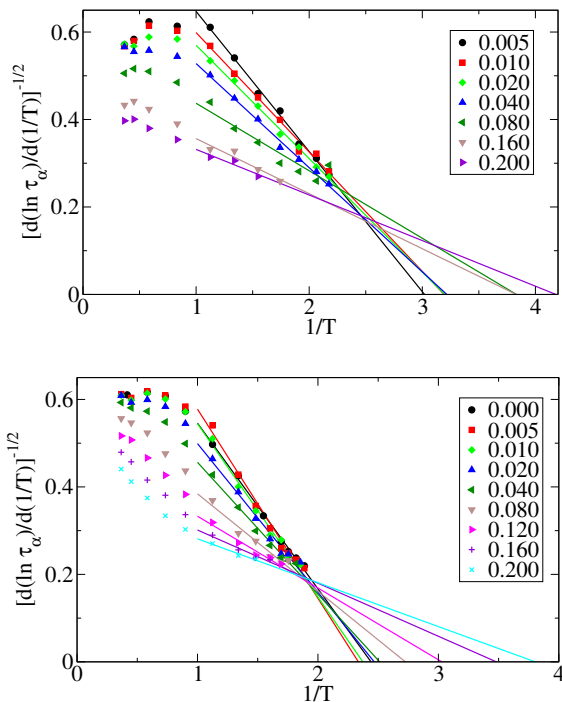


FIG. 8: Inverse temperature Stickel plots with linear fits in the region $T \leq 1$. *Left Panel:* 3dKA model. *Right Panel:* 3dR10 model. The x -intercepts give the values of $1/T_K$.

It is easy to see that

$$\Phi(T) = \sqrt{K_{VFT} T_K} \left(\frac{1}{T_K} - \frac{1}{T} \right), \quad (6)$$

if the VFT form holds. This implies that a plot of $\Phi(T)$ versus $1/T$ should be linear and extrapolate to zero at $1/T_K$. Thus T_K can be obtained from a linear fit to the $\Phi(T)$ versus $1/T$ data and the fragility parameter K_{VFT} can be obtained from the slope of the fitted straight line.

Stickel plots (plots of $\Phi(T)$ versus $1/T$) for the two model systems considered here are shown in Fig. 8. It is clear from these plots, even without doing any fitting, that the data for larger values of ρ_{pin} would extrapolate to zero at larger values of $1/T$, yielding lower values of T_K . This is precisely the trend observed in the values of T_K obtained from the VFT plots shown in the main paper. Also, the Stickel plots in Fig. 8 do not show any indication of this trend changing at still lower temperatures.

We fitted the low temperature parts ($T \leq 1$) of the $\Phi(T)$ data to straight lines to get T_K and K_{VFT} . These fits are shown in Fig. 8. The values obtained (shown in Fig. 9) agree with those obtained from our direct fits within error bars and show exactly the same general dependence on the pinning density.

- [1] W. Kob and H. C. Andersen, Phys. Rev. E **51**, 4626 (1995).
 [2] C. Cammarota and G. Biroli, Proc. Nat. Acad. Sci. **109**, 8850 (2012).

- [3] F. Stickel, E. W. Fischer and R. Richert, J. Chem. Phys., **102**, 6251, (1995).

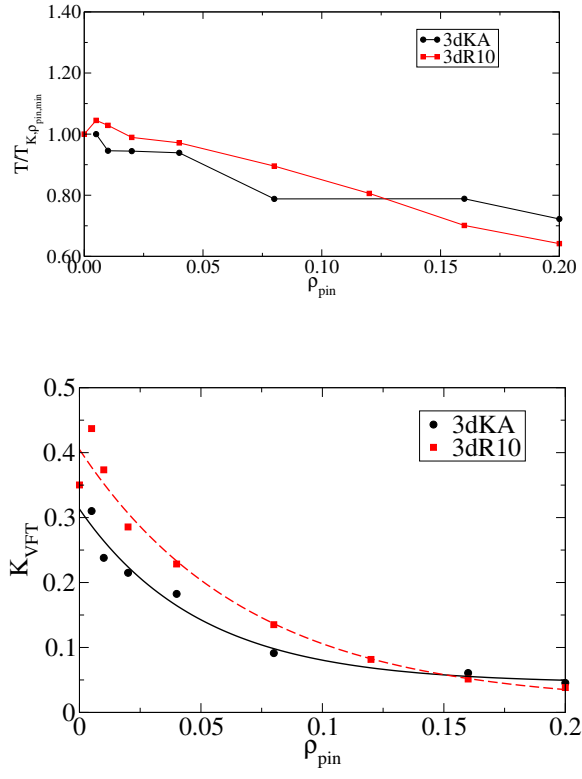


FIG. 9: Fit parameters obtained from fits in Fig. 8. *Left Panel: T_K . Right Panel: K_{VFT} .*